= const is a solution of Eq. (A12) corresponding to the eigenvalue $\gamma = 1$. We shall now show that there are no other solutions corresponding to eigenvalues of modulus unity. Let $y(t)$ be a solution of Eq. (A12) and ϕ_m be such that $|y(\phi_m)|$ is maximum. Then one can easily prove using Eq. (A12) that

$$|\gamma|\,|y(\phi_m)| \leq |y|_{\max'}, \qquad \text{(A13)}$$

where $|y|_{\max'}$ is the maximum value of $|y(\phi)|$ in the region of ϕ where $K(\phi_m, \phi)$ is different from zero. This region has been denoted by $d_1(\phi_m)$ previously [Eqs. (A2) and (A5)]. The equality in (A13) holds only if $y(\phi)$ is constant in $d_1(\phi_m)$. Thus, $|\gamma| < 1$ except if $y(\phi)$ is constant in $d_1(\phi_m)$ and such that $|y(\phi)| = |y(\phi_m)|$, $\phi \in d_1(\phi_m)$. In this last case one can repeat the argument taking as ϕ_m any point in $d_1(\phi_m)$. Then, it follows, using in addition the continuity of $d_1(\phi_m)$ that $|\gamma| < 1$ unless $y(\phi)$ is constant in $d_2(\phi_m)$ and such that $|y(\phi)| = |y(\phi_m)|$, $\phi \in d_2(\phi_m)$. Repeating the argument again and again we conclude that $|\gamma| < 1$, unless $y(\phi)$ is constant in every $d_j(\phi_m)$ ($j = 1, 2, 3, \ldots$). But we have shown that for large enough j, $d_j(\phi_m)$ coincides with the whole region $[-\frac{1}{2}\pi, \frac{1}{2}\pi]$. Thus $|\gamma| < 1$ unless $y(\phi)$ is constant everywhere.

*Work was completed when one of the authors (E.N.E.) was at the University of Virginia.

†Present address: Department of Physics, University of Virginia, Charlottesville, Va. 22901.

[1]D. S. Saxon and R. A. Hutner, Philips Res. Rept. 4, 81 (1949).

[2]J. M. Luttinger, Philips Res. Rept. 6, 303 (1951).

[3]H. M. James and A. S. Ginzbarg, J. Phys. Chem. 57, 840 (1953).

[4]R. Landauer and J. C. Helland, J. Chem. Phys. 22, 1655 (1954).

[5]M. Lax and J. C. Phillips, Phys. Rev. 110, 41 (1958).

[6]H. L. Frisch and S. P. Lloyd, Phys. Rev. 120, 1175 (1960).

[7]R. Eisenschitz and P. Dean, Proc. Phys. Soc. (London) 70, 713 (1957).

[8]H. Schmidt, Phys. Rev. 105, 425 (1957).

[9]N. F. Mott and W. D. Twose, Advan. Phys. 10, 107 (1961).

[10]R. E. Borland, Proc. Roy. Soc. (London) A274, 529 (1963).

[11]R. E. Borland and N. F. Bird, Proc. Phys. Soc. (London) 83, 23 (1964).

[12]B. I. Halperin, Advan. Chem. Phys. 13, 123 (1967).

[13]N. F. Mott, Advan. Phys. 16, 49 (1967).

[14]J. Hori, Progr. Theoret. Phys. (Kyoto) Suppl. 36, 3 (1966).

[15]E. N. Economou, M. H. Cohen, K. Freed, and S. Kirkpatrick (unpublished).

[16]E. H. Lieb and D. C. Mattis, *Mathematical Physics in One Dimension* (Academic, New York, 1966).

[17]J. Hori, *Spectral Properties of Disordered Chains and Lattices* (Pergamon, London, 1968).

[18]F. J. Dyson, Phys. Rev. 92, 1331 (1953).

[19]P. Dean, Proc. Roy. Soc. (London) 254, 507 (1960).

[20]J. Hori and M. Fukushima, J. Phys. Soc. Japan 19, 296 (1963).

[21]J. Hori and H. Matsuda, Progr. Theoret. Phys. (Kyoto) 32, 183 (1964).

[22]P. Dean, Proc. Phys. Soc. (London) 83, 591 (1964).

[23]P. W. Anderson, Phys. Rev. 109, 1492 (1958).

[24]E. N. Economou and Morrel H. Cohen (unpublished).

[25]E. N. Economou and Morrel H. Cohen, Phys. Rev. Letters 25, 1445 (1970).

[26]F. W. Williams and N. F. J. Mathews, Phys. Rev. 180, 864 (1969).

[27]E. N. Economou and Morrel H. Cohen, Phys. Rev. Letters 24, 218 (1970).

PHYSICAL REVIEW B VOLUME 4, NUMBER 2 15 JULY 1971

Optical Absorption of Sodium*

A. S. Karakashian† and A. Bardasis
Department of Physics and Astronomy, University of Maryland, College Park, Maryland 20742
(Received 21 December 1970)

The imaginary part of the transverse dielectric tensor has been calculated for sodium using a two-band model and including both phonons and the interactions between conduction electrons in the random-phase approximation. It is found that the resulting expression reduces to the Hopfield dielectric constant for the case of an electron gas in a perturbing crystal potential. Reasonable agreement with N. V. Smith's data has been found in the range of photon energies 0.5–3.0 eV. However, at higher energies the agreement is not as good, since many-body effects become more important in this region.

I. INTRODUCTION

In recent years it has become possible to measure the optical absorption of the alkali metals over a fairly large range of photon energies. Mayer and co-workers[1-3] performed a series of careful ab-

sorption experiments on the alkalis over photon energies 0.5–4 eV. The results were surprising because of the presence of an "anomalous" peak below the direct interband threshold. This peak was small in the case of sodium and appeared to be due to indirect (phonon-assisted) interband transitions. However, for potassium the anomalous peak was quite pronounced and seemed to be due to a mechanism other than indirect transitions. In order to verify the results of Mayer *et al.*, Smith[4] tried to reproduce the data for sodium and potassium. His data showed the presence of a direct interband peak, but no anomalous peak in the sodium and potassium absorption curves was found.

In spite of the discrepancies between the two experiments, many calculations have been performed in order to explain the data. One of the earliest computations of the direct interband absorption in the one-electron approximation was performed by Butcher.[5] When a realistic pseudopotential coefficient was used in his expression, the magnitude of the absorption did not agree with the experimental results. This suggested that the effects of the Coulomb interaction between electrons might be important in the optical absorption of the alkali metals.

Wolff[6] calculated the random-phase-approximation (RPA) correction to the optical conductivity of an electron gas using a statically screened Coulomb interaction and found that this correction vanished. Therefore, contributions to the optical absorption of the electron gas beyond the RPA had to be considered.

Both Overhauser[7] and Animalu[8] attempted to include collective effects by using an optical pseudopotential to compute the direct interband absorption of Bloch electrons. Since the effects of the phonons were neglected, these calculations had to be superimposed on a Drude background absorption in order to compare the results with the experimental data.

Hopfield[9] attempted to include lattice effects by choosing as a model for the solid an interacting electron gas in a perturbing crystal potential. Thus, he was able to show explicitly the dynamic screening of the electron-ion interaction by the longitudinal dielectric constant of the electron gas. However, the results did not differ significantly from Butcher's calculation when the Hartree dielectric constant was used for the screening.

Both Nettel[10] and Miskovsky and Cutler[11] performed calculations in the anomalous region by including the electron-phonon interaction to second order in perturbation theory. The results were in reasonably good agreement with Mayer's data for sodium below the direct interband threshold. Ferrell[12] pointed out, however, that Hopfield's formulation could be extended to include the indirect as well as the direct transitions. Therefore, the point of view of this paper will be to generalize Hopfield's results by considering a system of interacting Bloch electrons in a perturbing electron-phonon potential. The major emphasis will be on including the electron-phonon interaction and evaluating the optical matrix elements using a two-band model and the RPA for the electron-electron interactions.

II. FORMALISM

The starting point of the calculation is Pines's[13] form of the imaginary part of the transverse dielectric tensor for a cubic solid in the optical limit:

$$\mathrm{Im}\epsilon_{\nu\nu}(0,\omega) = (4\pi^2 e^2/\omega^2) \sum_n [\langle O|j_\nu^\dagger(0)|n\rangle \langle n|j_\nu(0)|O\rangle \times \delta(\omega-\omega_{n0}) - \langle O|j_\nu(0)|n\rangle \times \langle n|j_\nu^\dagger(0)|O\rangle\ \delta(\omega+\omega_{n0})] \ . \quad (2.1)$$

The νth component of the microscopic current operator is given by

$$j_\nu(0) = \sum_{i=1}^{N} \frac{P_{i\nu}}{m_0} \ , \quad (2.2)$$

and the optical matrix elements appearing in Eq. (2.1) are taken between the eigenstates of the Hamiltonian describing the solid:

$$H = H_e^B + H_I + H_{e\phi} \ , \quad (2.3a)$$

$$H_e^B = \sum_{i=1}^{N} \frac{P_i^2}{2m_0} + \sum_{i=1}^{N} V_{\text{lattice}}(\vec{r}_i) + \frac{1}{2} \sum_{i,j=1}^{N} V_c(\vec{r}_i - \vec{r}_j) \ , \quad (2.3b)$$

$$H_I = \sum_{\alpha=1}^{N} \frac{P_\alpha^2}{2M} + \frac{1}{2} \sum_{\alpha,\beta=1}^{N} V_c(\vec{R}_\alpha - \vec{R}_\beta) \ , \quad (2.3c)$$

$$H_{e\phi} = \sum_{i,\alpha=1}^{N} [U_0(\vec{r}_i - \vec{R}_\alpha) - \langle U_0(\vec{r}_i - \vec{R}_\alpha)\rangle_I] \ , \quad (2.3d)$$

where $(\vec{r}_i, \vec{p}_i)$ and $(\vec{R}_\alpha, \vec{P}_\alpha)$ are the positions and momenta of the ith electron and αth ion, respectively. The quantity $\langle U_0(\vec{r}_i - \vec{R}_\alpha)\rangle_I$ is the average of the electron-ion pseudopotential over the system of ions, and $\hbar\omega_{n0}$ is the energy difference between the nth excited state and the ground state of the Hamiltonian of the solid. In using Pines's form of the dielectric tensor, the induced electromagnetic fields have been neglected. Thus, the calculation only includes the response to the external field, as pointed out by Kadanoff and Martin.[14]

The Hopfield result can be obtained from Eq. (2.1) by assuming the following form for the Hamiltonian of an electron gas in a perturbing crystal potential:

$$H' = H_e^G + H_I + H_{eI} \ , \quad (2.4a)$$

$$H_e^G = \sum_{i=1}^{N} \frac{p_i^2}{2m_0} + \frac{1}{2} \sum_{i,j=1}^{N} V_c(\vec{r}_i - \vec{r}_j), \quad (2.4b)$$

$$H_{eI} = \sum_{i,\alpha=1}^{N} U_0(\vec{r}_i - \vec{R}_\alpha) , \tag{2.4c}$$

where H_I is defined by Eq. (2.3c). After the optical matrix elements in Eq. (2.1) are expanded to second order in the perturbing potential H_{eI}, they can be evaluated by making use of the fact that the eigenstates of the electron-gas Hamiltonian are also eigenstates of the current operator. The Hopfield dielectric constant can then be written in the form

$$\mathrm{Im}\epsilon_{\nu\nu}(0, \omega) = \frac{1}{m_0^2\omega^4}\int \frac{d^3\vec{q}}{(2\pi)^3}\left|\frac{\tilde{U}_0(\vec{q})}{\epsilon_{\mathrm{II}}(\vec{q}, \omega)}\right|^2 q^2 q_\nu^2 S_I(\vec{q})\,\mathrm{Im}\epsilon_{\mathrm{II}}(\vec{q}, \omega) , \tag{2.5}$$

where $\tilde{U}_0(\vec{q})$ is the Fourier transform of the electron-ion pseudopotential, $S_I(\vec{q})$ is the structure factor of the ion system, and $\epsilon_{\mathrm{II}}(\vec{q}, \omega)$ is the longitudinal dielectric constant of the electron gas. The dynamic screening of the electron-ion pseudopotential is explicitly displayed in Eq. (2.5)

The calculation of the dielectric constant of the solid described by Eqs. (2.3a)–(2.3d) proceeds basically as in the Hopfield case, except that $H_{e\phi}$ replaces H_{eI} and the states are interacting Bloch instead of electron-gas states. However, since Bloch states are not eigenstates of the current operator, the evaluation of the optical matrix elements in Eq. (2.1) becomes very difficult. One way to bypass this problem is to reformulate the expression for the dielectric constant so that a diagrammatic expansion of the matrix elements can be carried out. This method has two advantages. First, the diagrammatic technique facilitates the summation of a particular class of terms in a perturbation series. Second, this procedure involves the calculation of matrix elements between noninteracting Bloch states which can be approximated by the nearly-free-electron model. By using the integral representation of the energy δ functions appearing in Eq. (2.1) and the definition of the Heisenberg operators, the transverse dielectric tensor can be rewritten as

$$\mathrm{Im}\epsilon_{\nu\nu}(0, \omega) = (4\pi^2e^2/\omega^2)\,\mathrm{Re}[M_{\nu\nu}(0, \omega) - M_{\nu\nu}(0, -\omega)] , \tag{2.6a}$$

$$M_{\nu\nu}(0, \omega) = \int_0^\infty \frac{dt}{\pi} e^{i\omega t}\langle O|\, T(j_\nu(t)j_\nu^\dagger(0))\,|O\rangle , \tag{2.6b}$$

where $|O\rangle$ is the ground state of H, and T is the Wick time-ordering operator. The matrix elements in Eq. (2.6b) can now be expanded to second order in $H_{e\phi}$ by using the S-matrix formulation of perturbation theory and the linked-cluster theorem. After introducing the specific form of $H_{e\phi}$ the following expressions are obtained for the zeroth-, first-, and second-order contributions to the matrix element:

$$M_{\nu\nu}^{(0)}(0, \omega) = \int_0^\infty \frac{dt}{\pi} e^{i\omega t}\langle O_e^0|\, T(j_\nu(t)j_\nu^\dagger(0))\,S_{ee}\,|O_e^0\rangle_L , \tag{2.7a}$$

$$M_{\nu\nu}^{(1)}(0, \omega) = 0 , \tag{2.7b}$$

$$M_{\nu\nu}^{(2)}(0, \omega) = \int \frac{d^3q}{(2\pi)^3}\int \frac{d^3q'}{(2\pi)^3}\,\tilde{U}_0(\vec{q})\tilde{U}_0^*(\vec{q}') \times \int_{-\infty}^{\infty} d\Omega\, S_I(\vec{q}, \vec{q}', \Omega)\, XS_e(\vec{q}, \vec{q}', \Omega, \omega)_{\nu\nu} , \tag{2.7c}$$

where

$$\int_{-\infty}^{\infty} d\Omega e^{-i\Omega(t'-t'')} S_I(\vec{q}, \vec{q}', \Omega) = \langle O_I|\, T(\delta\rho_I(\vec{q}, t')\delta\rho_I^\dagger(\vec{q}', t''))\,|O_I\rangle , \tag{2.7d}$$

$$S_e(\vec{q}, \vec{q}', \Omega, \omega)_{\nu\nu} = \int_0^\infty \frac{dt}{2\pi} e^{i\omega t}\int_{-\infty}^{\infty} dt' \int_{-\infty}^{\infty} dt'' e^{-i\Omega(t'-t'')} \times \langle O_e^0|\, T(j_\nu(t)j_\nu^\dagger(0)\rho_e^\dagger(\vec{q}, t')\rho_e(\vec{q}', t''))\,S_{ee}\,|O_e^0\rangle_L . \tag{2.7e}$$

The states $|O_I\rangle$ and $|O_e^0\rangle$ are the ground states of H_I and H_0^B, respectively, where

$$H_0^B = \sum_{i=1}^{N} \frac{p_i^2}{2m_0} + \sum_{i=1}^{N} V_{\mathrm{lattice}}(\vec{r}_i) , \tag{2.8a}$$

$$H_{ee}(0) = \frac{1}{2}\sum_{i,j=1}^{N} V_c(\vec{r}_i - \vec{r}_j) , \tag{2.8b}$$

and

$$S_{ee} = P\exp[-i\int_{-\infty}^{\infty} d\xi\, H_{ee}(\xi)] . \tag{2.8c}$$

The density operators appearing in Eqs. (2.7d) and (2.7e) are the Heisenberg representations of

$$\delta\rho_I(\vec{q}) = \sum_{\alpha=1}^{N} [e^{-i\vec{q}\cdot\vec{R}_\alpha} - \langle e^{-i\vec{q}\cdot\vec{R}_\alpha}\rangle_I] \tag{2.9a}$$

and

$$\rho_e(\vec{q}) = \sum_{i=1}^{N} e^{-i\vec{q}\cdot\vec{r}_i} . \tag{2.9b}$$

The frequency integral over Ω in Eq. (2.7c) can be approximated in the following way. The ion form factor $S_I(\vec{q}, \vec{q}', \Omega)$ has its largest value when Ω is at the phonon frequency. Since the phonon frequency is much smaller than the optical frequency ω it can be neglected in the electron factor. Thus,

$$S_e(\vec{q}, \vec{q}', \Omega, \omega)_{\nu\nu} \approx S_e(\vec{q}, \vec{q}', 0, \omega)_{\nu\nu} , \tag{2.10}$$

and Eq. (2.7c) becomes

$$M_{\nu\nu}^{(2)}(0,\ \omega)=\int\frac{d^3q}{(2\pi)^3}\int\frac{d^3q'}{(2\pi)^3}\,\tilde{U}_0(\vec{q})\tilde{U}_0^*(\vec{q}\,')\times S_I(\vec{q},\ \vec{q}\,')S_e(\vec{q},\ \vec{q}\,',\ 0,\ \omega)_{\nu\nu}\ , \quad (2.11a)$$

where the structure factor is defined as

$$S_I(\vec{q},\ \vec{q}\,')=\int_{-\infty}^{\infty}d\Omega\,S_I(\vec{q},\ \vec{q}\,',\ \Omega)\ . \quad (2.11b)$$

The next step in the calculation is to replace the operators in Eqs. (2.7a) and (2.7e) by their second-quantized forms and expand the matrix elements by Wick's theorem. Therefore, a model for the lattice Green's function and ion factors used in the Wick expansion will be discussed in Sec. III.

III. MODELS

In order to compute the optical properties of the alkali metals, a two-band model must be used for the electrons because the photon energies are large enough to produce interband transitions. Therefore, in the reduced-zone scheme the one-electron Schrödinger equation is

$$H_0^B\psi_n(\vec{K},\ \vec{r})=\epsilon_n(\vec{K})\psi_n(\vec{K},\ \vec{r})\ , \quad (3.1a)$$

where $\vec{K}$ is the electron wave vector in the first Brillouin zone (BZ),

$$H_0^B=p^2/2m_0+V_{\vec{Q}}(e^{i\vec{Q}\cdot\vec{r}}+e^{-i\vec{Q}\cdot\vec{r}})\ , \quad (3.1b)$$

and $V_{\vec{Q}}$ is the lattice pseudopotential coefficient corresponding to the (110) reciprocal-lattice vector $\vec{Q}$. Since the wave function $\psi_n(\vec{K},\ \vec{r})$ is a Bloch wave, it can be expanded in terms of plane waves for a system of unit volume:

$$\psi_n(\vec{K},\ \vec{r})=\sum_{\vec{Q}_\alpha}\chi_n(\vec{K},\ \vec{Q}_\alpha)e^{i(\vec{K}+\vec{Q}_\alpha)\cdot\vec{r}}\ , \quad (3.2)$$

where $\vec{Q}_\alpha=\{0,\ \vec{Q}\}$. The wave-function coefficients $\chi_n(\vec{K},\ \vec{Q}_\alpha)$ have the well-known periodicity and completeness properties stated in Kittel.[15]

It is necessary to specify the wave-function coefficients and energy bands $\epsilon_n(\vec{K})$ in order to define the two-band model completely. There are two approximate solutions of Eq. (3.1a) which can be written in closed form. The perturbed-plane-wave (PPW) solution is obtained by assuming that $V_{\vec{Q}}$ is small and applying nondegenerate perturbation theory to solve the Schrödinger equation. This solution approximates the free-electron-like behavior of the real bands for small values of $\vec{K}$ but breaks down near the zone boundary. The nearly-free-electron model (NFE) makes use of degenerate perturbation theory to solve Eq. (3.1a) but gives results which approximate the real bands only for $\vec{K}$ values near the zone boundary where the energy gap occurs. Since phonons are present in the system, they can transfer large enough momenta to the electrons to excite them into states near the zone boundary. On the other hand, the photons have enough energy to excite electrons from states near the bottom of the band. Therefore, a composite model (CM) must be used which includes both the PPW and NFE models. An artificial cutoff wave vector K_0 is introduced, below which the PPW model is used and above which the NFE model is employed. The criterion used to determine K_0 is

$$\frac{G}{\epsilon_0(\vec{Q})}=\frac{|\tfrac{1}{2}\vec{Q}|-K_0}{|\tfrac{1}{2}\vec{Q}|}\ , \quad (3.3)$$

where G is the energy gap at the (110) face of the BZ and

$$\epsilon_0(\vec{Q})=\hbar^2|\vec{Q}|^2/2m_0\ . \quad (3.4)$$

The criterion was checked by using Ham's[16] band calculations for the alkali metals to estimate K_0 and comparing it to the value calculated from Eq. (3.3). The criterion was fairly well satisfied for all alkali metals except possibly rubidium and cesium. The value of K_0 calculated from Eq. (3.3) using 0.45 eV for the energy gap of sodium was 97.3% of $|\tfrac{1}{2}\vec{Q}|$.

In order to match the PPW wave functions and energies to the NFE values at K_0, a momentum-dependent lattice-pseudopotential coefficient is introduced,

$$V_{\vec{Q}}(\vec{K})=\begin{cases}V_{\vec{Q}} & |\vec{K}|>K_0\ (\text{NFE})\\ \tilde{V}_{\vec{Q}} & |\vec{K}|<K_0\ (\text{PPW})\end{cases}\ , \quad (3.5)$$

as well as the energy shifts E_n. The coefficient $V_{\vec{Q}}$ is determined by the energy gap G at the (110) face of the BZ,

$$|V_{\vec{Q}}|=\tfrac{1}{2}G\ . \quad (3.6)$$

The gap value of 0.45 eV for sodium results from an analysis by Ashcroft of Lee's[17] sodium data. The remaining pseudopotential coefficient is evaluated from the condition that $\chi_n(\vec{K},\ \vec{Q}_\alpha)$ be continuous at K_0. Similarly, the energy shifts E_n are calculated from the continuity condition on the band energies. The resulting composite model has one deficiency in that the slope of the energy is discontinuous at K_0. However, this is not a serious fault since the derivative of the energy bands is never used in the calculations, and the energy bands occur inside momentum integrals which average over the discontinuity in the derivative.

The lattice Green's function is defined as

$$G_0(\vec{r}\,t,\ \vec{r}\,'t')=-i\langle O_e^0|\,T(\psi(\vec{r}\,t)\psi^\dagger(\vec{r}\,'t'))\,|O_e^0\rangle\ , \quad (3.7)$$

where $\psi(\vec{r}\,t)$ is the field operator of an electron in the periodic lattice potential, T is the Wick time-

ordering operator, and $|O_e^0\rangle$ is the many-particle ground state of the noninteracting Bloch Hamiltonian H_0^B. Substituting the expansion of the field operators in terms of Bloch states into Eq. (3.7) results in the following form for the lattice Green's function:

$$G_0(\vec{r}t, \vec{r}'t') = \sum_{\vec{Q}_\alpha} \int_{\text{all } \vec{K}} \frac{d^3K}{(2\pi)^3} \int_{-\infty}^{\infty} \frac{d\omega}{2\pi} e^{i\vec{K}\cdot\vec{r}} e^{-i(\vec{K}+\vec{Q}_\alpha)\cdot\vec{r}'} \times e^{-i\omega(t-t')} G_0(\vec{K}, \vec{K}+\vec{Q}_\alpha, \omega), \quad (3.8a)$$

where

$$G_0(\vec{K}, \vec{K}+\vec{Q}_\alpha, \omega) = \sum_{n=1}^{2} \frac{\chi_n(\vec{K}, 0)\chi_n^*(\vec{K}, \vec{Q}_\alpha)}{\omega - \epsilon_n(\vec{K}) + i\delta_{n,\vec{K}}} . \quad (3.8b)$$

The notation $\delta_{n,\vec{K}}$ is defined in the two-band model as

$$\delta_{n,\vec{K}} = \begin{cases} +\delta \text{ if } n=2 \text{ or } n=1 \text{ and } |\vec{K}| > K_F \\ -\delta \text{ if } n=1 \text{ and } |\vec{K}| < K_F \end{cases} , \quad (3.8c)$$

where δ is an infinitesimal quantity and K_F is the Fermi wave vector. Notice that the electron momentum is not conserved by this propagator since the electron can pick up or lose a momentum $\hbar\vec{Q}_\alpha$ by interacting with the lattice. The wave-function coefficients and band energies appearing in Eq. (3.8b) are evaluated in the composite model defined above.

A simple model is adopted for the electron-ion pseudopotential which was used by Foo and Hopfield[18] in their calculation of the optical properties of alkalis. In this model only the s-wave component of the potential is retained. It is assumed that the conduction electron sees a constant potential inside a radius R of the equilibrium position of the ion and a Coulombic potential outside this radius. The radius parameter is a measure of the size of the ion and is determined by equating the ground-state energy to the experimental ionization energy. Therefore, the potential has the form

$$U_0(\vec{r}) = \begin{cases} -Z_e^2/r & \text{if } r > R \\ -Z_e^2/R & \text{if } r < R \end{cases} , \quad (3.9)$$

where Z is the valence of the ion and $R = 1.726$ Å for sodium. The Fourier transform of the model potential is

$$\tilde{U}_0(\vec{q}) = -(4\pi Ze^2/q^2)(\sin qR/qR) . \quad (3.10)$$

The dynamic form factor of the ion system is obtained by inverting the Fourier transform in the definition (2.7d). By interpreting the matrix element as a thermal average over the phonon-density correlations, the following result is obtained:

$$S_I(\vec{q}, \vec{q}', \Omega) = \frac{i}{4\pi M} \frac{(2\pi)^3}{V_0} e^{-[W(\vec{q},T)+W(\vec{q}',T)]} \times \sum_{p=1}^{3} \frac{[\vec{q}\cdot\vec{\epsilon}(p,\vec{q})][\vec{q}'\cdot\vec{\epsilon}^*(p,\vec{q})]}{\omega_0(p,\vec{q})} D_{0p}(\vec{q}, \Omega) \times \sum_{\vec{Q}_\alpha} \delta(\vec{q} - \vec{q}' - \vec{Q}_\alpha) , \quad (3.11a)$$

where V_0 is the volume of a unit cell. The bare-phonon propagator at finite temperature T and polarization p is given by

$$D_{0p}(\vec{q}, \Omega) = \frac{2\omega_0(p,\vec{q})\langle n(p,\vec{q}) + 1\rangle}{\Omega^2 - \omega_0^2(p,\vec{q}) + i\eta} - \frac{2\omega_0(p,\vec{q})\langle n(p,\vec{q})\rangle}{\Omega^2 - \omega_0^2(p,\vec{q}) - i\eta} , \quad (3.11b)$$

where $\omega_0(p,\vec{q})$ is the bare-phonon dispersion relation and $n(p,\vec{q})$ is the phonon number operator. The Debye-Waller factor appearing in Eq. (3.11a) is calculated from the expression

$$W(q, T) = \frac{V_0}{4M} \sum_{p=1}^{3} \int_{BZ} \frac{d^3f}{(2\pi)^3} \frac{|\vec{q}\cdot\vec{\epsilon}(p,\vec{f})|^2}{\omega_0(p,\vec{f})} \times \langle 2n(p,\vec{f}) + 1\rangle , \quad (3.11c)$$

where $\vec{\epsilon}(p,\vec{f})$ is the polarization vector of the phonons. The structure factor for this system was defined by Eq. (2.11b). The above expressions were derived within the single-phonon approximation. When these results are used in the calculation, it will be assumed that only phonons traveling in the [110] direction contribute; therefore, transverse phonons will not be included in the sum over polarizations in Eq. (3.11a).

IV. DIAGRAMS

The simplest contribution to the dielectric constant is the term which is zero order in the electron-ion interaction and given by Eqs. (2.6a) and (2.7a). When the matrix element is expanded by Wick's theorem, the result can be expressed diagrammatically as illustrated in Fig. 1. Only the RPA graphs to second order are shown. These diagrams can be evaluated by using the Feynman rules listed in the Appendix. However, the contributions from Figs. 1(b), 1(c), and higher order vanish be-

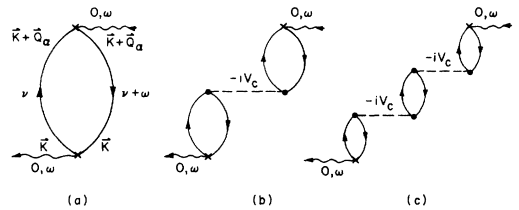

FIG. 1. (a) Basic polarization diagram for a periodic system which does not include phonons. (b) and (c) First- and second-order RPA corrections to (a).

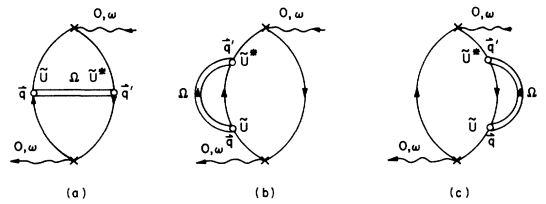

FIG. 2. Class-A diagrams which are second order in the screened electron-ion interaction. (a) Vertex correction; (b) and (c) self-energies due to the phonons.

cause only one electron-photon vertex appears in each bubble. Since each vertex introduces a factor K_ν into the momentum integral, the integrand is an odd function of the electron momentum for solids with inversion symmetry and vanishes when integrated over the Fermi sphere. As pointed out earlier, this result was obtained for the electron gas by Wolff. The graph in Fig. 1(a) is the only nonzero contribution in the RPA and gives essentially Butcher's result for the optical absorption due to direct interband transitions:

$$\mathrm{Im}\epsilon^{(0)}_{\nu,\nu'}(0,\omega)=\frac{4\pi^2e^2}{m_0^2\omega^2}\ \frac{2}{\pi}\ \mathrm{Re}\int\frac{d^3K}{(2\pi)^3}\int_{-\infty}^{\infty}\frac{d\nu}{2\pi}\sum_\alpha K_{\nu'}$$

$$\times(K_{\nu'}+Q_{\alpha\nu'})G_0(\vec{K},\vec{K}+\vec{Q}_\alpha,\nu)\,G_0(\vec{K}+\vec{Q}_\alpha,\vec{K},\ \nu+\omega). \tag{4.1}$$

The second-order term in the electron-ion interaction given by Eqs. (2.7e) and (2.11a) can be expanded similarly. Here, two classes of diagrams (classes A and B) are retained. The class-A diagrams are shown in Fig. 2. In this case the electron-electron interactions enter only through the screened electron-ion pseudopotential, as illustrated by the integral equations for the renormalized interactions in Fig. 3. These equations can be expressed in the following forms:

$$\tilde{U}(\vec{G}',\vec{q},\ \Omega)=\tilde{U}_0(\vec{G}')\,\delta(\vec{q}-\vec{G}')-iV_c(\vec{G}')$$

$$\times\sum_{\rho,\sigma}\tilde{P}^{\rho,\sigma}(\vec{G}',\Omega)\,\tilde{U}(\vec{G}'+\vec{Q}_\rho+\vec{Q}_\alpha,\vec{q},\Omega), \tag{4.2a}$$

where $\vec{G}'=\vec{q}'+\vec{Q}_\alpha+\vec{Q}_\beta+\vec{Q}_\gamma+\vec{Q}_\delta$, the pair bubble $\tilde{P}$ is given by

$$\tilde{P}^{\rho,\sigma}(\vec{G}',\Omega)=2\int\frac{d^3K}{(2\pi)^3}\int_{-\infty}^{\infty}\frac{d\nu}{2\pi}\,G_0(\vec{K},\vec{K}+\vec{Q}_\rho,\nu)$$

$$\times G_0(\vec{K}+\vec{G}'+\vec{Q}_\rho,\vec{K}+\vec{G}'+\vec{Q}_\rho+\vec{Q}_\alpha,\ \nu+\Omega), \tag{4.2b}$$

and the Fourier transform of the Coulomb interaction is

$$V_c(\vec{G}')=4\pi e^2/|\vec{G}'|^2. \tag{4.2c}$$

Similarly,

$$\tilde{U}^*(\vec{q}',\vec{G},\Omega)=\tilde{U}_0^*(\vec{G})\,\delta(\vec{G}-\vec{q}')-iV_c(\vec{G})$$

$$\times\sum_{\rho,\nu}P^{\rho,\sigma}(\vec{G},\Omega)\,\tilde{U}^*(\vec{q}',\vec{G}-\vec{Q}_\rho-\vec{Q}_\alpha,\Omega), \tag{4.3a}$$

where $\vec{G}=\vec{q}-\vec{Q}_\alpha-\vec{Q}_\beta-\vec{Q}_\gamma-\vec{Q}_\delta$ and the pair bubble P is defined by

$$P^{\rho,\sigma}(\vec{G},\Omega)=2\int\frac{d^3K}{(2\pi)^3}\int_{-\infty}^{\infty}\frac{d\nu}{2\pi}\,G_0(\vec{K},\vec{K}+\vec{Q}_\rho,\nu)$$

$$\times G_0(\vec{K}+\vec{G}-\vec{Q}_\alpha,\vec{K}+\vec{G},\ \nu+\Omega). \tag{4.3b}$$

Since Eqs. (4.2a) and (4.3a) are in general two infinite sets of algebraic equations coupled by the reciprocal-lattice vectors, they cannot conveniently be solved unless a two-band model is used. In this case the solutions can be expressed as

$$\tilde{U}(\vec{q}'+\vec{Q}_\alpha,\vec{q},\Omega)=\frac{\tilde{U}_0(\vec{q})}{\epsilon_{\parallel}(\vec{q},\Omega)}\,\delta(\vec{q}-\vec{q}'-\vec{Q}_\alpha) \tag{4.4a}$$

and

$$\tilde{U}^*(\vec{q}',\vec{q}-\vec{Q}_\alpha,\Omega)=\frac{\tilde{U}_0^*(\vec{q}')}{\epsilon_{\parallel}(\vec{q}',\Omega)}\,\delta(\vec{q}-\vec{q}'-\vec{Q}_\alpha), \tag{4.4b}$$

where $\vec{Q}_\alpha=\{0,\vec{Q}\}$ and the longitudinal dielectric constant $\epsilon_{\parallel}(\vec{q},\Omega)$ is

$$\epsilon_{\parallel}(\vec{q},\Omega)=1+i\,V_c(\vec{q})\,\tilde{P}^{0,0}(\vec{q},\Omega)$$

$$=1+i\,V_c(\vec{q})\,P^{0,0}(\vec{q},\Omega). \tag{4.4c}$$

Now the contribution of the class-A diagrams to the second-order term in the transverse dielectric tensor can be obtained by combining Eqs. (2.6a), (2.11a), (4.4a), and (4.4b). Therefore,

$$\mathrm{Im}\epsilon^{(2)}_{\nu\nu}(0,\omega)=\frac{4\pi^2e^2}{\omega^2}\int\frac{d^3q}{(2\pi)^3}\int\frac{d^3q'}{(2\pi)^3}\,\frac{\tilde{U}_0(\vec{q})}{\epsilon_{\parallel}(\vec{q},0)}\,\frac{\tilde{U}_0^*(\vec{q}')}{\epsilon_{\parallel}(\vec{q}',0)}$$

$$\times S_I(\vec{q},\vec{q}')\,\mathrm{Re}[S_e^A(\vec{q},\vec{q}',0,\omega)_{\nu\nu}-S_e^A(\vec{q},\vec{q}',0,-\omega)_{\nu\nu}], \tag{4.5}$$

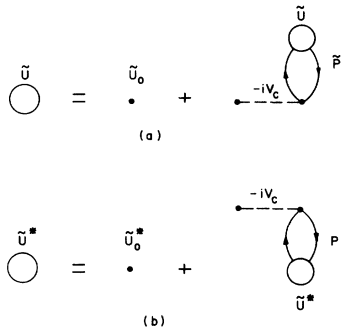

FIG. 3. Representations of the integral equations for the outgoing and incoming screened electron-ion vertices.

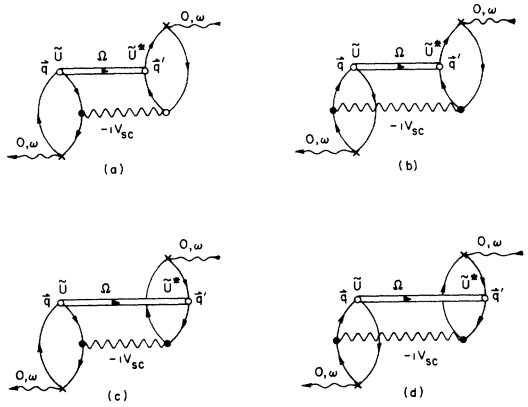

FIG. 4. Class-B diagrams with screened Coulomb interactions. These diagrams are responsible for the dynamic screening of the electron-ion interaction in the limit of a translationally invariant system.

where the notation S_e^A means that only class-A diagrams are included in the electron factor in the square bracket. It should be noted that the class-A diagrams produce a static screening of the electron-ion pseudopotential.

The class-B diagrams shown in Fig. 4 must also be included in Eq. (2.7e) in order to obtain a result which reduces to the Hopfield dielectric constant in the limit of a translationally invariant system. The electron-electron interactions occur in both the screened electron-ion vertices and the screened-Coulomb-interaction line between the pair loops. The screened Coulomb interaction can be obtained from the integral equation represented pictorially in Fig. 5. The corresponding expression is

$$-iV_{sc}(\vec{G},\vec{G}',\omega) = -iV_c(\vec{G})\,\delta(\vec{G}-\vec{G}') - iV_c(\vec{G})\sum_{\lambda,\pi} P^{\lambda,\pi}(\vec{G},\omega)[-iV_{sc}(\vec{G}-\vec{Q}_\lambda-\vec{Q}_\pi,\vec{G}',\omega)], \tag{4.6}$$

where $\vec{G}=\vec{q}-\vec{Q}_\beta-\vec{Q}_\gamma-\vec{Q}_\delta$, $\vec{G}'=\vec{q}'+\vec{Q}_\sigma+\vec{Q}_\eta+\vec{Q}_\rho$, and the pair bubble $P^{\lambda,\pi}$ was previously defined in Eq. (4.3b). Notice that the momentum of the photons corresponding to the screened Coulomb propagator is not conserved but can change by a reciprocal-lattice vector. Now the two-band model is used to solve the coupled set of equations (4.6):

$$V_{sc}(\vec{q}-\vec{Q}_\alpha,\vec{q}'+\vec{Q}_\beta,\omega) = \frac{V_c(\vec{q}-\vec{Q}_\alpha)}{\epsilon_{II}(\vec{q}-\vec{Q}_\alpha,\omega)}\,\delta(\vec{q}-\vec{q}'-\vec{Q}_\alpha-\vec{Q}_\beta), \tag{4.7}$$

where $\vec{Q}_\alpha=\{0,\vec{Q}\}$ and $\vec{Q}_\beta=\{0,\vec{Q}\}$. The contribution of the class-A and -B graphs to the second-order term can now be written within the two-band model as

$$\mathrm{Im}\epsilon_{\nu\nu}^{(2)}(0,\omega)=\frac{4\pi^2e^2}{\omega^2}\int\frac{d^3q}{(2\pi)^3}\int\frac{d^3q'}{(2\pi)^3}\,\frac{\tilde{U}_0(\vec{q})}{\epsilon_{II}(\vec{q},0)}\,\frac{\tilde{U}_0^*(\vec{q}')}{\epsilon_{II}(\vec{q}',0)} \times S_I(\vec{q},\vec{q}')\,\mathrm{Re}[S_e^{A+B}(\vec{q},\vec{q}',0,\omega)_{\nu\nu} - S_e^{A+B}(\vec{q},\vec{q}',0,-\omega)_{\nu\nu}], \tag{4.8a}$$

where

$$S_e^{A+B}(\vec{q},\vec{q}',0,\omega)_{\nu',\nu'}=\frac{1}{m_0^2}\sum_{\alpha\beta\gamma\delta}\int d^3\vec{k}\int_{-\infty}^{\infty}\frac{d\nu}{2\pi} \times\delta(\vec{q}-\vec{q}'-\vec{Q}_\alpha-\vec{Q}_\beta-\vec{Q}_\gamma-\vec{Q}_\delta)\,(K_{\nu'}+Q_{\alpha\nu})G_0(\vec{K},\vec{K}+\vec{Q}_\alpha,\nu)\,G_0(\vec{K}+\vec{Q}_\alpha,\vec{K}+\vec{Q}_\alpha+\vec{Q}_\beta,\nu+\omega) \times[(K_{\nu'}+q_{\nu'}-Q_{\delta\nu})\,G_0(\vec{K}+\vec{q}-\vec{Q}_\gamma-\vec{Q}_\delta,\vec{K}+\vec{q}-\vec{Q}_\delta,\nu+\omega)\,G_0(\vec{K}+\vec{q}-\vec{Q}_\delta,\vec{K}+\vec{q},\nu)+K_{\nu'}\,G_0(\vec{K}-\vec{Q}_\gamma,\vec{K},\nu+\omega) \times G_0(\vec{K}+\vec{q}-\vec{Q}_\gamma-\vec{Q}_\delta,\vec{K}+\vec{q}-\vec{Q}_\gamma,\nu+\omega)+(K_\nu+Q_{\alpha\nu}+Q_{\beta\nu})\,G_0(\vec{K}+\vec{Q}_\alpha+\vec{Q}_\beta,\vec{K}+\vec{Q}_\alpha+\vec{Q}_\beta+\vec{Q}_\gamma,\nu) \times G_0(\vec{K}+\vec{q}+\vec{Q}_\alpha+\vec{Q}_\beta+\vec{Q}_\gamma,\vec{K}+\vec{q}+\vec{Q}_\alpha+\vec{Q}_\beta+\vec{Q}_\gamma+\vec{Q}_\delta,\nu)] - [iV_c(\vec{q})/\epsilon_{II}(\vec{q},\omega)]\,\delta(\vec{q}-\vec{q}')\,[P_\nu(\vec{q},0,\omega)]^2 \tag{4.8b}$$

and

$$P_{\nu'}(\vec{q},0,\omega)=\frac{2i}{m_0}\int\frac{d^3K}{(2\pi)^3}\int_{-\infty}^{\infty}\frac{d\nu}{2\pi}\,K_\nu\,G_0(\vec{K},\vec{K},\nu) \times G_0(\vec{K},\vec{K},\nu+\omega)\,G_0(\vec{K}+\vec{q},\vec{K}+\vec{q},\nu+\omega)\,. \tag{4.8c}$$

If the system is translationally invariant, as in the

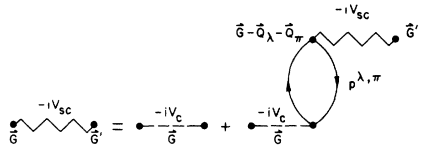

FIG. 5. Representation of the integral equation for the dynamic Coulomb interaction in a periodic system.

Hopfield case, the lattice Green's functions in Eq. (4.8b) are replaced by

$$G_0(\vec{K}, \nu) = \frac{n(\vec{K})}{\nu - \epsilon_0(\vec{K}) - i\delta} + \frac{1 - n(\vec{K})}{\nu - \epsilon_0(\vec{K}) + i\delta} \quad , \tag{4.9a}$$

where

$$n(\vec{K}) = \begin{cases} 1 & \text{if } |\vec{K}| < K_F \\ 0 & \text{if } |\vec{K}| > K_F \end{cases} . \tag{4.9b}$$

The replacement leads to the following result for the electron factor:

$$S_e^{A+B}(\vec{q}, \vec{q}', 0, \omega)_{\nu\nu} = \frac{q_\nu^2}{m_0^2\omega^2} [P(\vec{q}, \omega) - P(\vec{q}, 0)] \delta(\vec{q} - \vec{q}')$$

$$+ \frac{q_\nu^2}{m_0^2\omega^2} \frac{-iV_c(\vec{q})}{\epsilon_{\parallel}(\vec{q}, \omega)} [P(\vec{q}, \omega) - P(\vec{q}, 0)]^2 \delta(\vec{q} - \vec{q}') , \tag{4.10a}$$

where

$$P(\vec{q}, \omega) = 2i \int \frac{d^3K}{(2\pi)^3} n(\vec{K})[1 - n(\vec{K} + \vec{q})]$$

$$\times \left(\frac{1}{\omega - \epsilon_0(\vec{K}) - \epsilon_0(\vec{K} + \vec{q}) + i\delta} - \frac{1}{\omega + \epsilon_0(\vec{K} + \vec{q}) - \epsilon_0(\vec{K}) - i\delta} \right) . \tag{4.10b}$$

Taking the real part of Eq. (4.10a) gives

$$\mathrm{Re} S_e^{A+B}(\vec{q}, \vec{q}', 0, \omega)_{\nu\nu}$$

$$= \frac{q_\nu^2}{m_0^2\omega^2} \delta(\vec{q} - \vec{q}') \left| \frac{\epsilon_{\parallel}(\vec{q}, 0)}{\epsilon_{\parallel}(\vec{q}, \omega)} \right|^2 \mathrm{Re} P(\vec{q}, \omega) . \tag{4.10c}$$

When Eq. (4.10c) is substituted into Eq. (4.8a), the Hopfield dielectric constant as given in Eq. (2.5) is obtained. Notice that the dynamic screening replaces the static screening only because of the special simplifications which occur in the translationally invariant case. Namely, the dielectric tensor can only depend on q_ν^2 in the Hopfield system, whereas the periodic system contains the reciprocal-lattice vector $\vec{Q}$ and thus the dielectric tensor can be expressed as a linear combination of

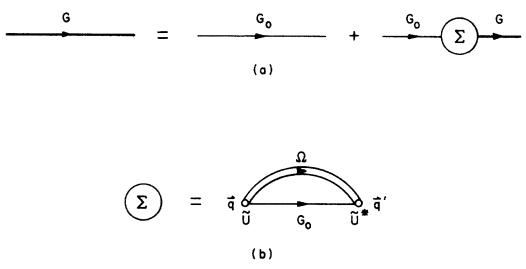

FIG. 6. (a) Dyson equation for the renormalized lattice Green's function; (b) lowest-order contribution of the phonons to the self-energy.

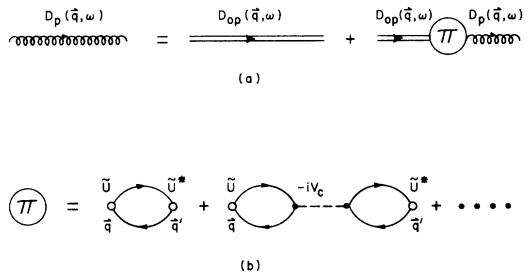

FIG. 7. (a) Dyson equation for the renormalized phonon propagator; (b) first two terms in the expansion of the Coulomb contribution to the self-energy.

all products of q_ν and Q_ν. Thus, there are static as well as dynamically screened terms in the dielectric tensor of the periodic system.

Up to this point, only second-order electron-ion interactions have been taken into account in the transverse dielectric tensor. It has been shown that the class-A and -B terms reduce to the Hopfield result for a translationally invariant system. Now the above results will be extended to higher order in the electron-ion pseudopotential by including the phonon contribution to the self-energy of the particle propagator. Furthermore, the phonon propagator will also be renormalized, and the zero-order class-A and -B diagrams will be recalculated.

In Fig. 6(a) the Dyson equation for the lattice Green's function is shown. Since the electron-ion vertex appears at least to second order in the self-energy in Fig. 6(b), the umklapp term with $\vec{q}' = \vec{q} - \vec{Q}$ will be neglected compared to the normal term, i.e.,

$$\frac{\tilde{U}_0(\vec{q} - \vec{Q}) S_I(\vec{q}, \vec{q} - \vec{Q})}{\tilde{U}_0(\vec{q}) S_I(\vec{q}, \vec{q})} < 1 \quad . \tag{4.11}$$

Therefore, the renormalized lattice Green's functions can be approximated by

$$G(\vec{K}, \vec{K}, \nu) = \frac{G_0(\vec{K}, \vec{K}, \nu)}{1 - \Sigma(\vec{K}, \nu) G_0(\vec{K}, \vec{K}, \nu)} , \tag{4.12a}$$

$$G(\vec{K} + \vec{Q}, \vec{K}, \nu) = G_0(\vec{K} + \vec{Q}, \vec{K}, \nu), \tag{4.12b}$$

$$G(\vec{K}, \vec{K} + \vec{Q}, \nu) = G_0(\vec{K}, \vec{K} + \vec{Q}, \nu) , \tag{4.12c}$$

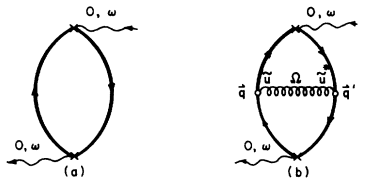

FIG. 8. Renormalized zero-order (a) and vertex (b) diagrams which correspond to Figs. 1(a) and 2(a).

where

$$\Sigma(\vec{K},\nu)=i\int\frac{d^3q}{(2\pi)^3}\left|\frac{\tilde{U}_0(\vec{q})}{\epsilon_{11}(\vec{q},0)}\right|^2\int_{-\infty}^{\infty}d\Omega\,S_I(\vec{q},\vec{q},\Omega)$$

$$\times G_0(\vec{K}+\vec{q},\vec{K}+\vec{q},\nu+\Omega). \qquad (4.12d)$$

Since the optical properties are of primary interest here, a separate calculation of the phonon contribution to the self-energy including the effects of periodicity will not be done. Instead, Schrieffer's[19] evaluation of the imaginary part of the self-energy of an electron gas will be used, and the real part will be neglected in order to facilitate the numerical calculations. The imaginary part of the self-energy gives rise to a finite lifetime for an electron or hole because of the possibility of decay by the emission or absorption of a phonon:

$$\mathrm{Im}\Sigma(K_F,\nu)^D=\Gamma(\nu)$$

$$=\begin{cases}\frac{1}{3}(4/9\pi)^{1/3}r_s\Omega_p[(\nu-\epsilon_F)/\Omega_p]^3, & \nu\le\epsilon_F+\Omega_p\\ \frac{1}{3}(4/9\pi)^{1/3}r_s\Omega_p, & \nu>\epsilon_F+\Omega_p\end{cases} \qquad (4.13)$$

where Ω_p is the ion-plasma frequency and r_s is given by $(4\pi/3)\,r_s^3a_0^3=1/n_e$, where n_e is the electron density and a_0 is the Bohr radius.

The Dyson equation and the corresponding self-energy for the phonon propagator are shown in Figs. 7(a) and 7(b). The net effect of including the self-energy in the phonon Green's function is to replace the bare-phonon spectrum $\omega_0(p,\vec{q})$ by the real-phonon spectrum $\omega(p,\vec{q})$ in the denominator of the longitudinal-phonon propagator, as pointed out by Schrieffer[19]:

$$D_{11}(\vec{q},\Omega)=\frac{2\omega_{011}(\vec{q})\,\langle n_{11}(\vec{q})+1\rangle}{\Omega^2-\omega_{11}^2(\vec{q})+i\eta}$$

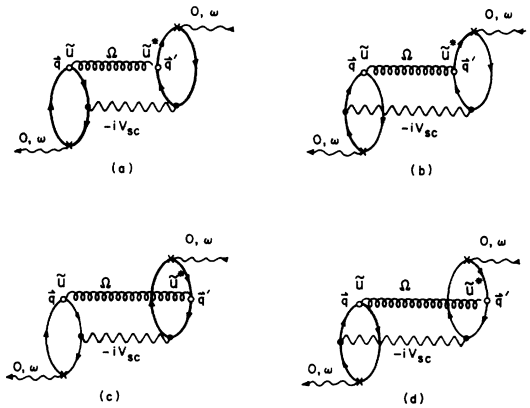

FIG. 9. Renormalized class-B diagrams which correspond to Fig. 4.

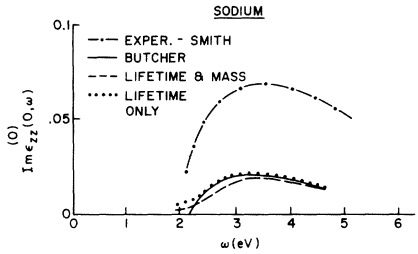

FIG. 10. Plot of $\mathrm{Im}\epsilon^{(0)}$ vs ω for Na at 293 °K showing the effects of various approximations for the self-energy on the direct interband absorption.

$$-\frac{2\omega_{011}(\vec{q})\langle n_{11}(\vec{q})\rangle}{\Omega^2-\omega_{11}^2(\vec{q})-i\eta}\ , \qquad (4.14a)$$

where

$$\omega_{11}(\vec{q})=\omega_{011}(\vec{q})/[\epsilon_{11}(\vec{q},0)]^{1/2}. \qquad (4.14b)$$

Now the previous results will be recalculated using the renormalized propagators in the zero-order diagram of Fig. 1(a), the bare-vertex diagram of Fig. 2(a), and the class-B diagrams of Fig. 4. The corresponding renormalized graphs are illustrated in Figs. 8 and 9. Note that the self-energy diagrams of Figs. 2(b) and 2(c) are not recalculated since they are already included in the renormalized zero-order graph. After substituting the new propagators and performing the frequency integral in Eq. (4.1), the phonon contribution to Butcher's result is obtained:

$$\mathrm{Im}\epsilon_{\nu\nu}^{(0)}(0,\omega)=\frac{4\pi^2e^2}{m_0^2\omega^2}\int_{K<K_F}\frac{d^3K}{(2\pi)^3}\,|\chi_1(\vec{K},0)|^2\,|\chi_2(\vec{K},0)|^2$$

$$\times\left\{K_\nu^2\left[\frac{\Gamma/\pi}{[\omega+\epsilon_1(\vec{K})-\epsilon_2(\vec{K})]^2+\Gamma^2}-\delta(\omega+\epsilon_1(\vec{K})-\epsilon_2(\vec{K}))\right]\right.$$

$$\left.-K_\nu Q_\nu\,\delta[\omega+\epsilon_1(\vec{K})-\epsilon_2(\vec{K})]\right\}. \qquad (4.15)$$

Note that the δ-function terms are produced by the umklapp term of the lattice Green's function, while the Lorentzian is due to the normal term. The numerical results of this expression are shown in Fig. 10 and discussed more fully in Karakashian and Bardasis.[20]

The vertex diagram of Fig. 8(b) can be separated into various terms according to the type of transition to which they contribute. After the frequency integral in Eq. (4.8b) is evaluated, the transitions can be identified by inspecting the form of the energy-conserving δ functions or Lorentzians. These transitions are labeled process 1, 2, or 3. Process

1 is a direct interband transition, process 2 is an indirect (phonon-assisted) transition, and process 3 is an intraband transition. The three processes are illustrated in Fig. 11. Thus the final form of the renormalized "second-order" dielectric tensor can be written as

$$\mathrm{Im}\epsilon_{\nu\nu}^{(2)}(0,\omega)=\frac{4\pi^2e^2}{m_0^2\omega^2}\int\frac{d^3\vec{q}}{(2\pi)^3}\left\{\left|\frac{\tilde{U}_0(\vec{q})}{\epsilon_{\parallel}(\vec{q},0)}\right|^2 S_I(\vec{q},\vec{q})\,\mathrm{Re}\left[\sum_{p=1}^{3}S_e^{(P)}(q,q,0,\omega)_{\nu\nu}-\frac{iV_c(\vec{q})}{\epsilon_{\parallel}(\vec{q},\omega)}P_\nu^2(\vec{q},0,\omega)\right]\right.$$

$$\left.+\frac{\tilde{U}_0(\vec{q})}{\epsilon_{\parallel}(\vec{q},0)}\,\frac{\tilde{U}_0^*(\vec{q}-\vec{Q})}{\epsilon_{\parallel}(\vec{q}-\vec{Q},0)}\,S_I(\vec{q},\vec{q}-\vec{Q})\sum_{p=1}^{3}\mathrm{Re}\,S_e^{(P)}(\vec{q},\vec{q}-\vec{Q},0,\omega)_{\nu\nu}\right\},\qquad(4.16a)$$

where

$$P_\nu(\vec{q},0,\omega)=2iq_\nu\sum_{j,m=1}^{2}\int\frac{d^3K}{(2\pi)^3}\,n_1(1-n_m')\frac{1}{\omega+\epsilon_1-\epsilon_m'+i\Gamma(1+\delta_{m,1})}\,\frac{|\chi_1(\vec{K},0)|^2|\chi_j(\vec{K}+\vec{q},0)|^2|\chi_m(\vec{K}+\vec{q},0)|^2}{\epsilon_1-\epsilon_j'}\,.\qquad(4.16b)$$

The prime on a quantity means that the argument of the quantity is $\vec{K}+\vec{q}$, whereas unprimed quantities have argument $\vec{K}$. The electron factors are given by the following expressions:

$$\mathrm{Re}S_e^{(1)}(\vec{q},\vec{q},0,\omega)_{\nu\nu}=2\int\frac{d^3K}{(2\pi)^3}\,n_1(1-n_2)\,\frac{\Gamma/\pi}{(\omega+\epsilon_1-\epsilon_2)^2+\Gamma^2}$$

$$\times\left[\frac{T_{\nu\nu}^{1211}(N)+\tilde{T}_{\nu\nu}^{1121}(N)}{(\epsilon_1'-\epsilon_1)(\epsilon_1'-\epsilon_2)}+\frac{T_{\nu\nu}^{1221}(N)+\tilde{T}_{\nu\nu}^{1221}(N)}{(\epsilon_1'-\epsilon_1)(\epsilon_2'-\epsilon_2)}+\frac{T_{\nu\nu}^{1212}(N)+\tilde{T}_{\nu\nu}^{2121}(N)}{(\epsilon_2'-\epsilon_1)(\epsilon_1'-\epsilon_2)}+\frac{T_{\nu\nu}^{1222}(N)+\tilde{T}_{\nu\nu}^{2221}(N)}{(\epsilon_2'-\epsilon_1)(\epsilon_2'-\epsilon_2)}\right],\qquad(4.17a)$$

$$\mathrm{Re}S_e^{(2)}(\vec{q},\vec{q},0\ \omega)_{\nu\nu}=-2\int\frac{d^3K}{(2\pi)^3}\,n_1(1-n_2')\,\frac{\Gamma/\pi}{(\omega+\epsilon_1-\epsilon_2')^2+\Gamma^2}$$

$$\times\left[\frac{T_{\nu\nu}^{1121}(N)+\tilde{T}_{\nu\nu}^{1211}(N)}{(\epsilon_1'-\epsilon_1)(\epsilon_2'-\epsilon_1)}+\frac{T_{\nu\nu}^{1222}(N)+\tilde{T}_{\nu\nu}^{2221}(N)}{(\epsilon_2'-\epsilon_1)(\epsilon_2'-\epsilon_2)}+\frac{T_{\nu\nu}^{1221}(N)+\tilde{T}_{\nu\nu}^{1221}(N)}{(\epsilon_1'-\epsilon_1)(\epsilon_2'-\epsilon_2)}+\frac{T_{\nu\nu}^{1122}(N)+\tilde{T}_{\nu\nu}^{2211}(N)}{(\epsilon_2'-\epsilon_1)^2}\right],\qquad(4.17b)$$

and

$$\mathrm{Re}S_e^{(3)}(\vec{q},\vec{q},0\ \omega)_{\nu\nu}=-2\int\frac{d^3K}{(2\pi)^3}\,n_1(1-n_1')\,\frac{2\Gamma/\pi}{(\omega+\epsilon_1-\epsilon_1')^2+4\Gamma^2}$$

$$\times\left[\frac{T_{\nu\nu}^{1111}(N)+\tilde{T}_{\nu\nu}^{1111}(N)}{(\epsilon_1'-\epsilon_1)^2}+\frac{T_{\nu\nu}^{1212}(N)+\tilde{T}_{\nu\nu}^{2121}(N)}{(\epsilon_2'-\epsilon_1)(\epsilon_1'-\epsilon_2)}+\frac{T_{\nu\nu}^{1211}(N)+\tilde{T}_{\nu\nu}^{1121}(N)}{(\epsilon_1'-\epsilon_1)(\epsilon_1'-\epsilon_2)}+\frac{T_{\nu\nu}^{1112}(N)+\tilde{T}_{\nu\nu}^{2111}(N)}{(\epsilon_2'-\epsilon_1)(\epsilon_1'-\epsilon_1)}\right].\qquad(4.17c)$$

The index p in Eq. (4.16a) specifies the process, while N or U indicates a normal or umklapp term. The umklapp terms have the same form as the corresponding normal terms given in Eqs. (4.17a)–(4.17c), except that the Lorentzians are replaced by δ functions. The terms in the second square brackets are the optical matrix elements, where the momentum tensors in the numerators are defined as

$$T_{\nu\nu}^{jlmn}(\alpha,\beta,\gamma,\delta)=(K_\nu+Q_{\alpha\nu})(K_\nu+q_\nu-Q_{\beta\nu})\,\chi_j(\vec{K},0)\chi_j^*$$

$$\times(\vec{K},\vec{Q}_\alpha)\,\chi_l(\vec{K},\vec{Q}_\alpha)\,\chi_l^*(\vec{K},\vec{Q}_\alpha+\vec{Q}_\beta)\,\chi_m(\vec{K}+\vec{q},\ -\vec{Q}_\gamma-\vec{Q}_\delta)$$

$$\times\chi_m^*(\vec{K}+\vec{q},-\vec{Q}_\delta)\,\chi_n(\vec{K}+\vec{q},-\vec{Q}_\delta)\,\chi_n^*(\vec{K}+\vec{q},0)\qquad(4.18a)$$

and

$$\tilde{T}_{\nu\nu}^{jlmn}(\alpha,\beta,\gamma,\delta)=(K_\nu+q_\nu+Q_{\alpha\nu})(K_\nu-Q_{\beta\nu})\,\chi_j(\vec{K}+\vec{q},0)$$

$$\times\chi_j^*(\vec{K}+\vec{q},\vec{Q}_\alpha)\,\chi_l(\vec{K}+\vec{q},\vec{Q}_\alpha)\,\chi_l^*(\vec{K}+\vec{q},\vec{Q}_\alpha+\vec{Q}_\beta)$$

$$\times\chi_m(\vec{K},-\vec{Q}_\gamma-\vec{Q}_\delta)\,\chi_m^*(\vec{K},-\vec{Q}_\delta)\,\chi_n(\vec{K},-\vec{Q}_\delta)\,\chi_n^*(\vec{K},0).\qquad(4.18b)$$

In the normal terms, all reciprocal-lattice vectors in Eqs. (4.18a) and (4.18b) are set equal to zero. For the umklapp terms the momentum tensors are evaluated by adding together all terms where all but one of the reciprocal-lattice vectors are zero. Recall that it was the difficulty in calculating the

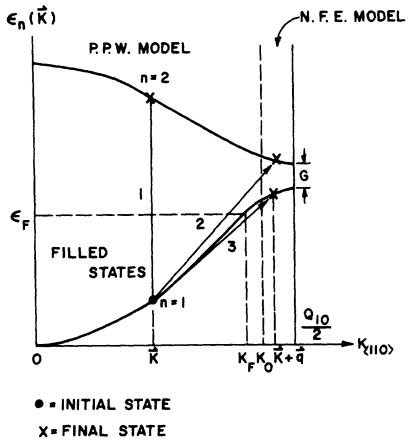

FIG. 11. Schematic representation of the three transitions which can occur in a periodic system including phonons. Process 1 is a direct interband transition. Process 2 is an indirect (or phonon-assisted) interband transition, and process 3 is an intraband (or Drude) transition.

optical matrix elements for a periodic system which led to the diagrammatic formulation. It has been found in Eqs. (4.17a)–(4.17c) that these matrix elements can be expressed in terms of momentum tensors made up of all possible products of any two vectors $\vec{K}$, $\vec{q}$, or $\vec{Q}$ weighted by the wave-function coefficients of the intermediate as well as the initial and final states. Since the wave-function coefficient $|\chi_n(\vec{K}, \vec{Q}_\alpha)|^2$ represents the probability that a state of wave vector $\vec{K}$ in band n has a momentum $\hbar(K+Q_\alpha)$, the above results make sense physically.

V. NUMERICAL CALCULATIONS AND RESULTS

The final form of the transverse dielectric tensor is

$$\mathrm{Im}\epsilon^{\perp}_{\nu\nu}(0,\omega) = \mathrm{Im}\epsilon^{(0)}_{\nu\nu}(0,\omega) + \mathrm{Im}\epsilon^{(2)}_{\nu\nu}(0,\omega)\ , \quad (5.1)$$

where the first term is given by Eq. (4.15) and the second term by Eq. (4.16a). The ion structure factor which appears in the latter equation is to be evaluated by Eqs. (3.11a) and (3.11b), where the real-phonon spectrum replaces the bare spectrum because the dressed-phonon propagators are used in the diagrams. The complicated nature of the remaining momentum integrals requires the use of numerical techniques for their evaluation. The Gaussian quadrature method was used for the integrations rather than Simpson's rule, since this method gives convergent results for a relatively small number of points. The convergence of the integrals was checked by increasing the number of points and comparing the result to the original value of the integral.

Several approximations have been made in connection with the self-energy. These approximations were checked by calculating their effects on $\mathrm{Im}\epsilon^{(0)}_{\nu\nu} \times(0,\omega)$. First, the zero-order term was calculated from Eq. (4.1), which contains no self-energy effects. This is the solid curve of Fig. 10 and is essentially the same as Butcher's calculation for the interband absorption. Then Eq. (4.5) was used to compute the zero-order term, thus including the imaginary part of the self-energy only. This is the dotted curve of Fig. 10. Finally, the real as well as the imaginary part of the self-energy was included by using the value of Ashcroft and Wilkins, [21] $m_0/m^* = 0.847$, for the effective mass in sodium. This gives the dashed curve of Fig. 10. The inclusion of the effective mass reduces the peak absorption by about 15% and shifts the peak position by less than 0.5 eV in addition to smearing out the threshold.

The constant lifetime approximation for the imaginary part of the self-energy was used since only high-energy optical excitations were calculated. It can be seen from Eq. (4.13) that this is a good approximation in the optical region. In the infrared range where the excitation energy is smaller, this approximation breaks down. However, the calculation is not good in this region anyhow since the phonon energy was neglected compared to the optical excitation energy in the electron factors. As a result, the real part of the conductivity becomes infinite at zero excitation energy ω instead of approaching its dc value.

The theoretical results which have been obtained are compared to Smith's[4,22] data in Fig. 12 for sodium. The results are in general agreement with Smith's data in the range of photon energies 0.5–3.0 eV. However, the structure due to the phonon-assisted transitions at about 1.0 eV is not present in

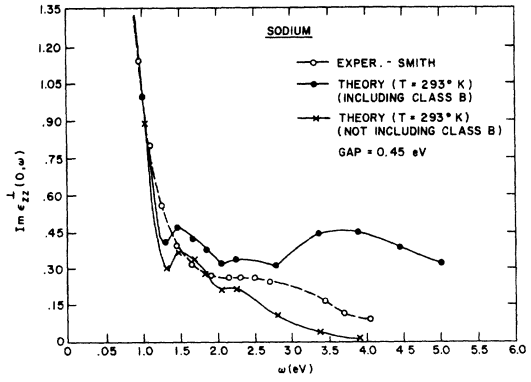

FIG. 12. Plot of the theoretical curves of $\mathrm{Im}\epsilon^{\perp}$ vs ω for Na at 293 °K compared to Smith's data. The upper curve shows the absorption due to the renormalized zero-order class-A vertex and class-B diagrams. The middle curve displays Smith's experimental values, and the lower curve shows the effect of not including the class-B diagrams.

the data because of the difficulty in resolving this peak experimentally. The direct interband peak is barely resolved in the data and coincides with the theoretical threshold. The reason for the agreement in this region is that the combination of intraband and indirect interband absorption falls less rapidly than the background calculated from the simple Drude formula. Since previous calculations of the direct interband absorption were superimposed on the Drude background, the results for sodium were too small by as much as 50%. Between 3.0 and 4.0 eV the theoretical curve departs radically from the experimental values. The deviation is due to a broad plasmonlike peak occurring above 3.0 eV eV, which is produced by the class-B (or dynamic screening) term. When the class-B term is removed, the absorption drops off faster than the experimental curve, as shown in Fig. 12. This indicates two things: First, the Coulomb interactions between conduction electrons tend to raise the absorption at the higher frequencies, and second, the class-B term alone is not sufficient to give the correct results above 3.0 eV. In order to obtain better agreement with experiment in the range of photon energies above 3.0 eV, it is necessary to include vertex, self-energy, and possibly ladder-type graphs in the Coulomb interaction, as indicated in a paper by Bardasis and Hone[23] on the many-body effects in semiconductors. Thus, the main emphasis should be placed on evaluating the optical matrix elements in the two-band model near the thresholds for processes 1 and 2; however, above the direct interband threshold, the Coulomb interactions must be taken into account more carefully.

ACKNOWLEDGMENTS

The authors wish to express their thanks to Dr. David S. Falk for suggesting this problem and for many critical discussions of this work. We also are indebted to Dr. Arnold J. Glick for his helpful recommendations concerning the phonon self-energy effects. The computer time for this project was supported in full through the facilities of the Computer Science Center of the University of Maryland.

APPENDIX: FEYNMAN RULES IN MOMENTUM SPACE

Dielectric constant:

$$\mathrm{Im}\epsilon_{\nu\nu}(0,\ \omega) = (4\pi^2 e^2/\omega^2)\ \mathrm{Re}[M_{\nu\nu}(\omega) - M_{\nu\nu}(-\omega)]\ , \tag{A1}$$

where the matrix elements are given by

$$M_{\nu\nu}(\omega) = \sum_{i=1}^{\infty} G_i \tag{A2}$$

and G_i is a linked graph. The rules for contributions from graphs G_i are

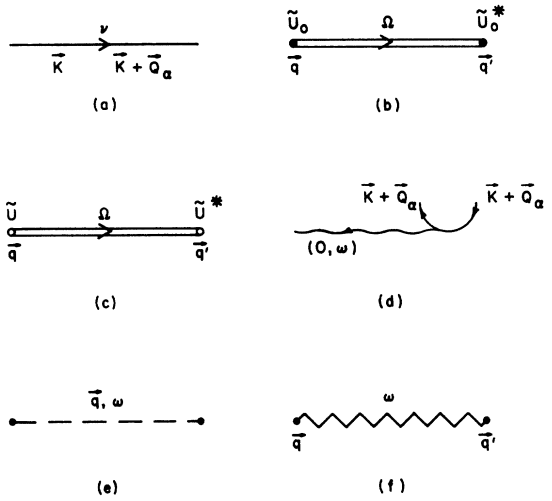

FIG. 13. Feynman graphs for various interaction lines.

factor of $(-2)^L/2\pi$, (A3)

where L is the number of closed particle loops and 2 is the spin factor.

For each particle line, as in Fig. 13(a), there is a factor

$$iG_0(\vec{K},\ \vec{K}+\vec{Q}_\alpha,\ \nu)\ . \tag{A4}$$

For each phonon line with bare electron-ion interactions at the ends, as in Fig. 13(b), there is a factor

$$\tilde{U}_0(\vec{q})\tilde{U}_0^*(\vec{q}')S_I(\vec{q},\ \vec{q}',\ \Omega)\ . \tag{A5}$$

For each phonon line with screened electron-ion interaction at the ends, as in Fig. 13(c), there is a factor

$$\frac{\tilde{U}_0(\vec{q})}{\epsilon_{\mathrm{II}}(\vec{q},\ \Omega)}\ \frac{\tilde{U}_0^*(\vec{q}')}{\epsilon_{\mathrm{II}}(\vec{q}',\ \Omega)}\ S_I(\vec{q},\ \vec{q}',\ \Omega)\ . \tag{A6}$$

For each electron-phonon vertex, as in Fig. 13(d), there is a factor

$$(K_\nu + Q_{\alpha\nu})/m_0\ . \tag{A7}$$

For each bare-Coulomb-interaction line, as in Fig. 13(e), there is a factor

$$-iV_c(\vec{q})\ . \tag{A8}$$

For each screened-Coulomb-interaction line, as in Fig. 13(f), there is a factor

$$-iV_{sc}(\vec{q},\ \vec{q}',\ \omega)\ . \tag{A9}$$

Conserve energy and momentum at each vertex using $(2\pi)^3$ times a momentum δ function at the last vertex encountered to force momentum conservation. (A10)

Sum over all reciprocal-lattice vectors and integrate over all internal momenta and energies:

$$\sum_{\alpha} \int \frac{d^3K}{(2\pi)^3} \int_{-\infty}^{\infty} \frac{d\nu}{2\pi} . \tag{A11}$$

---

*Supported in part by Advanced Research Project Agency ONR and U. S. Air Force Office of Scientific Research; Submitted by A. S. Karakashian in partial fulfillment of the Ph. D. degree in physics at the University of Maryland.

†Present address: Department of Physics, Lowell Technological Institute, Lowell, Mass.

[1]H. Mayer and M. H. El Naby, Z. Physik 174, 269 (1963).

[2]H. Mayer and B. Hietel, in *Optical Properties and Electronic Structure of Metals and Alloys*, edited by F. Abeles (North-Holland, Amsterdam, 1966), p. 47.

[3]J. N. Hodgson, in Ref. 2, p. 60.

[4]N. V. Smith, Phys. Rev. Letters 21, 96 (1968).

[5]P. N. Butcher, Proc. Phys. Soc. (London) A64, 765 (1951).

[6]P. A. Wolff, Phys. Rev. 116, 544 (1959).

[7]A. W. Overhauser, Phys. Rev. 156, 844 (1967).

[8]A. O. E. Animalu, Phys. Rev. 163, 557 (1967); 163, 562 (1967).

[9]J. J. Hopfield, Phys. Rev. 139, A419 (1965).

[10]S. J. Nettel, Phys. Rev. 150, 421 (1966).

[11]N. M. Miskovsky and P. H. Cutler, Department of Physics Report, University of Pennsylvania, 1969 (unpublished).

[12]R. A. Ferrell, in Ref. 2, p. 78.

[13]D. Pines, *Elementary Excitations in Solids* (Benjamin, New York, 1963), p. 199.

[14]L. P. Kadanoff and P. C. Martin, Phys. Rev. 124, 670 (1961).

[15]C. Kittel, *Introduction to Solid State Physics* (Wiley, New York, 1966), pp. 253–264.

[16]F. S. Ham, Phys. Rev. 128, 82 (1962).

[17]M. J. G. Lee, Proc. Roy. Soc. (London) A295, 440 (1966).

[18]E-Ni Foo and J. J. Hopfield, Phys. Rev. 173, 635 (1968).

[19]J. R. Schrieffer, *Superconductivity* (Benjamin, New York, 1964), p. 156.

[20]A. S. Karakashian and A. Bardasis, Phys. Letters 32A, 17 (1970).

[21]N. W. Ashcroft and J. W. Wilkins, Phys. Letters 14, 285 (1965).

[22]N. V. Smith, Phys. Rev. 163, 552 (1967).

[23]A. Bardasis and D. Hone, Phys. Rev. 153, 849 (1967).